Two Dimensional Generalized Edge Detector

Binnur Kurt, Muhittin Gökmen
Computer Engineering Department
İstanbul Technical University, Maslak, İstanbul, 80626, TURKEY
{kurt,gokmen}@cs.itu.edu.tr

Abstract

Detecting edges in images is one of the most challenging issue in computer vision and image processing due to lack of a robust detector. Gökmen and Jain [1] have obtained an edge detector called Generalized Edge Detector (GED), capable of producing most of the existing edge detectors. The original problem was formulated on two dimensional Hybrid model [1] comprised of the linear combination of membrane and thin-plate functionals. Smoothing problem was then reduced to the solution of two dimensional partial differential equation (PDE). The filters were obtained for one dimensional case assuming a seperable solution.

This study extends edge detection of images in $\lambda\tau$-space to two dimensional space. Two dimensional extension of the representation is important since the properties of images in the space is best modeled by two dimensional smoothing and edge detector filters. Also since GED filters encompass most of the well-known edge detectors, two dimensional version of these filters could be obtained. The derived filters are more robust to noise when compared to the previous one dimensional filtering scheme in the sense of FOM (Figure Of Merit), missing and false alarm characteristics. Experimental results on synthetic and natural images are presented, including an analysis of the introduced two dimensional edge detector filters and the behaivor of the detected edges through the $\lambda\tau$-space.

1 Introduction

The aim of edge detection is to provide a meaningful description of object boundaries in a scene from intensity surface. These boundaries are due to discontinuities manifesting themselves as sharp variations in image intensities. There are different sources for sharp changes in images which are created by structure (e.g. texture, occlusion) or illumination (e.g. shadows, highlights). Extracting edges from a still image is certainly the most significant stage of any computer vision algorithm requiring high accuracy of location in the presence of noise. In many contour-based vision algorithms, such as shape-based query, curved-based stereo vision, and edge-based target recognition, their performance is highly dependent on the quality of the detected edges. Therefore, edge detection is an important area of research in computer vision. Despite considerable work and progress made on this subject, edge detection is still a challenging research problem due to the lack of a robust and efficient general purpose algorithm.

Most of the efforts in edge detection have been devoted to the development of an optimum edge detector which can resolve the tradeoff between good localization and detection performance ([2, 3, 4, 5]). Furthermore, extracting edges at different scales ([2, 3, 6]) and combining these edges ([3, 7]) have attracted a substantial amount of interest. In the course of developing optimum edge detectors that can resolve the tradeoff between localization and detection performances, several different approaches have resulted in either a Gaussian filter or a filter whose shape is very similar to a Gaussian ([2, 3, 8]). Furthermore, these filters are very suitable for obtaining scale space edge detection since the scale of the filter can be easily controlled by means of a single parameter. Although these filters are used very widely, it is very difficult to claim that they can provide the desired output for any specific problem. For instance, there are some cases where the improved localization performance is the primary requirement. In these cases, a sub-optimum filter which promotes the localization performance becomes more appropriate. It has been shown that the first order R-filter can deliver improved results on checkerboard and bar images as well as some real images for moderate values of signal-to-noise ratio (SNR) [7]. In many vision applications, there is a great demand for a general-purpose edge detector which can produce edge maps with very different characteristics in nature, so that one of these edge maps may meet the requirements of the problem under consideration.

We begin this paper with an overview of the Hybrid model and the $\lambda\tau$-space representation of images and edges. Then we derive the two dimensional smoothing (R-filter) and edge detector (G-filter) filters in Section 3. Algorithm

implementation on synthetic and natural data is presented in Section 4. Finally, we conclude in Section V.

2 The Hybrid Model and $\lambda\tau$-Space Representation

In the course of developing the generalized edge detector, the authors in [1] explored the relationship between regularization theory and convolution with filters. Regularization theory is a general framework used to convert an ill-posed problem to well-posed by restricting the class of admissible solutions using the constraints such as smoothness ([9]). The smoothness can be imposed on the solution by minimizing an energy functional containing derivatives of the solution. Given noisy data $d(x, y)$, the regularized solution $f(x, y)$ can be found by minimizing

$$E_m(f) = \int\int_\Omega [|f - d|^2 + \lambda \|\nabla f\|^2] d\Omega \tag{1}$$

where $E_m(f)$ is the energy functional associated with membrane. Another energy functional used to obtain a regularized solution contains the second derivatives of the solution. In this case, a problem is posed finding an f that minimizes

$$E_p(f) = \int\int_\Omega [|f - d|^2 + \lambda \|\mathcal{H} f\|^2] d\Omega \tag{2}$$

where $E_p(f)$ is the energy functional associated with thin plate. In these functionals, the first term on the right hand side is a measure of closeness of the solution $f(x, y)$ to the data $d(x, y)$, and the second term, stabilizer, is a measure of the smoothness. Here $\mathcal{H}$ is the Hessian operator. The compromise between these two terms is controlled by the regularization parameter λ.

It was shown that ([7, 10]) a multiscale representation can be obtained by carrying out the smoothing process using regularization instead of filtering with a Gaussian. Each level of resolution is obtained by minimizing, for example, the functional (1). The scale parameter, in this case, is the regularization parameter λ, so that the coarse levels of representation are obtained by minimizing the membrane functional with a large λ, while fine levels are obtained by using a small λ. A multiscale edge representation can be obtained by locating the local maxima in the magnitude of the gradient of these regularized solutions.

The relationship between the regularization and filtering process is established by solving the Euler-Lagrange equation associated with the functional. Let us consider the membrane functional. The associated Euler-Lagrange equation will be as follows

$$f - \lambda \Delta f = d \tag{3}$$

with the boundary conditions $\lim_{x,y\to\pm\infty} f(x, y) = 0$. Suppose that the solution of the PDE given above is denoted by the function $R(x, y)$ when $d(x, y) = \delta(x, y)$. For given any $d(x, y)$, the solution $f(x, y)$ can be easily determined by taking the convolution as follows

$$f(x, y) = d(x, y) * R(x, y) \tag{4}$$

The properties of R-filters for membrane and thin plate functionals are given in [1] in detail. The goal of the hybrid model is to provide the smooth transitions between these two groups of filters. For this purpose, linear combination of the membrane and the thin plate functionals is obtained as follows

$$E_h(f) = \int\int_\Omega [|f - d|^2 + \lambda((1-\tau)\|\nabla f\|^2 + \tau\|\mathcal{H} f\|^2)] d\Omega \tag{5}$$

where λ is the real-valued regularization parameter and $\tau \in [0, 1]$ is the real-valued continuity control parameter. Here, the hybrid functional is used to obtain a smooth transition from membrane model to the plate model. Note that, for $\tau = 0$, the functional reduces to the membrane model, for $\tau = 1$ it reduces to the plate model, and for intermediate values of this parameter we obtain hybrid surfaces. In order to find a smooth transition between two filter groups, we need the solution of the Euler-Lagrange eqution associated to the hybrid functional. In the next section, the R-filter corresponding to the hybrid functional will be derived and analyzed.

3 Derivation of Two Dimensional R- and G-Filters

We now consider the hybrid energy functional and try to find out a function $f(x, y)$ minimizing the functional. As a first step, we obtain the Euler-Lagrange equation associated with the hybrid functional

$$f(x, y) - Q\triangle f(x, y) + P\triangle^2 f(x, y) = d(x, y) \tag{6}$$

on $\Omega = \{(x, y) | x \geq 0, y \geq 0\}$ where $Q = \lambda(1 - \tau)$ and $P = \lambda\tau$ with the mixed boundary conditions

$$\lim_{x,y\to\infty} f(x, y) = 0, \ \lim_{x,y\to 0} \nabla f = \mathbf{0} \tag{7}$$

and

$$\int\int_\Omega f(x, y) dx dy = 1.$$

The partial differential equation (6) can be written in terms of differential operators as

$$\mathcal{L} f = d \tag{8}$$

$$\mathcal{L} = P\triangle^2 - Q\triangle + 1 \tag{9}$$

The differential operator, $\mathcal{L}$, can be composed as

$$\begin{aligned} \mathcal{L} &= P\mathcal{L}_1\mathcal{L}_1 \\ \mathcal{L}_1 &= (\triangle - \eta) \\ \mathcal{L}_2 &= (\triangle - \xi) \end{aligned} \tag{10}$$

where η and ξ are the roots of the polynomial, $Ps^2 - Qs + 1 = 0$. Here, the operators $\mathcal{L}_1$ and $\mathcal{L}_2$ are the PDE's of Helmholtz type and its solution is given in [11]. Four cases may occur with respect to $P = 0$ and the sign of $\Delta = Q^2 - 4P$. The values of η and ξ are given in Table 1 for these cases. The corresponding solutions (R-filter) of the PDE (6) are given in Table 2. The G-filter is obtained by taking the derivative of R-filter with respect to x and y. G-filter along x direction denoted by $G^{(x)}(x, y)$ is given in Table 3. Note that the R-filters are symmetric while the G-filters are antisymmetric. Both filters do not have circular symmetry as contrary to Gaussian filter. Fig. 1 shows the R-filter $R(x, y; \lambda, \tau)$ for the specified values of λ and τ. The parameter values and the corresponding cases are shown in Table 4. Although only nine discrete values of the parameters are used, the above formulation allows us to obtain the $R(x, y; \lambda, \tau)$ and $G(x, y; \lambda, \tau)$ filters as λ and τ values vary continuously in the range $\lambda > 0$ and $0 \leq \tau \leq 1$. The curve with $\lambda\tau/(1-\tau)^2 = 4$ derived from $\Delta = 0$ divides the space, limited by $\tau = 0$ (the membrane model) and $\tau = 1$ (the plate model) lines, into two regions, say Regions I and II. The analysis of this space reveals that the shape of the filter does not change as we move along any $\lambda\tau/(1-\tau)^2 = constant$ curve. On the other hand, moving across these curves will considerably change the shape of the corresponding filter. One of the important differences between filters in Region I and in Region II is that the R-filter does not have negative values for any λ and τ in Region I, where as it will have two negative lobes at both sides of the central positive lobe for λ and τ in Region II. These negative values are the primary reasons for the overshoots around discontinuities at the filtered images. Thus one can observe that in Region I, the first order R-filter is gradually transformed to a Gaussian-like filter as τ increases while in region II, the Gaussian-like filter is transformed to the second order R-filter as τ increases.

4 Experimental Results

Does the hybrid model provide any improved results as compared to the membrane and plate functionals? To answer this question we consider a checkerboard image and then analyze the reconstructed images obtained with $\tau = 0,\ 0.5$ and 1, which are shown in Fig. 2. We see that each model has its own difficulty in reconstructing the original image. On the other hand, the hybrid solution obtained with $\tau = 0.5$ does not suffer from oversmoothed discontinuities of the membrane solution or the overshoots of the plate solution. As compared to these two standard models, the hybrid model provides a better replica of the original surface. In order to evaluate the reconstructed surfaces quantitatively, we calculate the mean square error ($nmse$) between the original image and the reconstructed image, shown in Table 5. The hybrid model results in a smaller $nmse$ as compared to the membrane and plate model for the moderate λ values, while the $nmse$ value is the smallest for the membrane model for large λ values in which case none of the results are satisfactory. The quantitative and qualitative results show experimentally that improved results may be obtained by means of the hybrid model with $0 < \tau < 1$ and it justifies sweeping of τ values between 0 and 1 as well as sweeping λ in continuum to obtain the so called $\lambda\tau$-*space representation* of images.

In order to expose the properties of the generalized edge detection algorithm and the advantages of using such a filter for different purposes, we have considered two different set of images. The first set of images consists of noisy checkerboard and bar images. These synthetic images are useful to determine how well the detector can handle the tradeoff between the detection and localization performances and to evaluate the results quantitatively as well. The $\lambda\tau$-space edge representations for the checkerboard image are shown in Fig. 3. To quantitatively evaluate the results, we calculated the conditional probability of a detected edge pixel given an ideal edge pixel, $P(DE/IE)$, the conditional probability of an ideal edge pixel given a detected edge pixel, $P(IE/DE)$, the Pratt's Figure Of Merit (FOM), and the mean square distance (MSD) between ideal and detected edge pixels [7]. Edge detectors should maximize the probability measures $P(DE/IE)$ and $P(IE/DE)$ as well as FOM while minimizing the error distance. The quantitative results are shown in Table 6 where the best result are obtained for $\lambda = 16$ and $\tau = 0$ values. As another test image, we have considered the noisy house image in Fig. 4 where the standard deviation of the additive Gaussian noise is 80. The $\lambda\tau$-space edge representation obtained with the generalized edge detector is shown in Fig. 5. In this case, the first-order R-filter results in noisy edge fragments as shown in the left column. Note that even with a large value of the smoothing parameter λ, these noisy and disconnected edges can not be eliminated. For this image, the edges obtained with $\tau = 0.5$ and $\lambda = 16$ are better. These two examples show that different problems require different edge detectors and the generalized edge detector is capable of producing these different results as samples of the scale-continuity ($\lambda\tau$) space representation.

5 Summary and Conclusion

We have presented two dimensional edge detector by using the hybrid model derived from the membrane and

plate models. Compared to the scale space representation, this representation can decompose the image/surface into a larger number of descriptions, each of which exhibits different characteristics of the image or surface.

After finding the relationship between the minimization of the hybrid functional and convolution of an image with a filter, we can regard this representation as an extended scale space representation where the shape characteristic of the filter as well as its scale change. The hybrid model and the edge detection have been examined on various types of data obtained from different cues. We have experimentally shown that the hybrid model provides additional information compared to the two extreme constituent models, *i.e.*, the membrane and plate models. We believe that the proposed representation will be applicable to a wide variety of problems.

We have derived a general-purpose edge detector from the hybrid model, which encompasses most of the well-known edge detectors under a unified framework. The edge representation generated by this operator contains very different edge descriptions, so the desired edge description required for a given problem can be found in this representation. We believe that this generalization and flexibility is very suitable for developing successful vision systems and that the generalized edge detector will find many applications.

Table 1. Values of η and ξ for four cases.

Case		η	ξ
I	$\Delta > 0$	$\frac{Q+\sqrt{\Delta}}{2P}$	$\frac{Q-\sqrt{\Delta}}{2P}$
II	$\Delta < 0$	$\frac{Q+i\sqrt{\lvert\Delta\rvert}}{2P}$	$\frac{Q-i\sqrt{\lvert\Delta\rvert}}{2P}$
III	$\Delta = 0$	$\frac{Q}{2P}$	$\frac{Q}{2P}$
IV	$P = 0$	$\frac{1}{Q}$	-

Table 2. R-filters

Case		$R(x,y)$
I	$\Delta > 0$	$\frac{2P}{\sqrt{\Delta}}[a\exp(-b(\lvert x\rvert+\lvert y\rvert))-$ $b\exp(-a(\lvert x\rvert+\lvert y\rvert))]$, $a=\sqrt{\frac{Q+\sqrt{\Delta}}{4P}}$, $b=\sqrt{\frac{Q-\sqrt{\Delta}}{4P}}$
II	$\Delta < 0$	$K\exp(-\frac{1}{\sqrt[4]{4P}}\cos(\theta)(\lvert x\rvert+\lvert y\rvert))\times$ $(\sin\theta+\varphi(\lvert x\rvert+\lvert y\rvert)$ $K=\frac{4}{\sqrt{P}\cos^3(\theta)\sin^2(2\theta)}$, $2\theta=\arctan\frac{\sqrt{\lvert\Delta\rvert}}{Q}$, $\varphi=\frac{1}{\sqrt[4]{4P}}\sin(\theta)$
III	$\Delta = 0$	$\frac{1}{4Q}(\frac{1}{\sqrt{Q}}\lvert x\rvert+1)(\frac{1}{\sqrt{Q}}\lvert y\rvert+1)$ $\exp(-\sqrt{\frac{1}{Q}}(\lvert x\rvert+\lvert y\rvert))$
IV	$P = 0$	$2Q\exp(-\sqrt{\frac{1}{2Q}}(\lvert x\rvert+\lvert y\rvert))$

References

[1] M. Gökmen and A.K. Jain,"$\lambda\tau$-Space Representation of Images and Generalized Edge Detector," IEEE Trans. on Pattern Analysis and Machine Intelligence, vol.9, pp. 545-563, 1997.

[2] D. Marr and E. Hildreth, "Theory of Edge Detection," Proceedings of Roy. Soc., (Sec B,207), pp.187-217, 1980.

[3] J.F. Canny, "A Computational Approach to Edge Detection," IEEE Trans. On Pattern Analysis and Machine Intelligence, Vol. 8, pp. 679-698, 1986.

[4] R. Deriche, "Optimal Edge Detection using Recursive Filtering," Proc. IEEE First International Conference on Computer Vision, pp. 501-505, 1987.

[5] J. Shen and S. Castan, "An Optimal Linear Operator for Edge Detection," Proc. IEEE First Conference on Pattern Recognition, pp. 109-114, 1986.

[6] A.P. Witkin, "Scale-space Filtering," Proc. 8th Int. Joint Conf. on Artificial Intelligence, pp. 1019-1022, 1983.

[7] M. Gökmen and C. Li, "Multiscale Edge Detection using first-order R-filter," Proc. Int. Conf. Pattern Recognition, pp. 307-310, 1992.

[8] T. Poggio, H. Voorhees, and A. Yuille, "A Regularized Solution to Edge Detection," Technical Report, MIT AI Lab., AI Memo 833, 1985.

[9] M. Bertero, T. Poggio, and V. Torre, "Ill-posed Problems in Early Vision," Technical Report, MIT AI Lab., AI Memo 924, 1987.

[10] A. Blake and A. Zisserman, Visual Reconstruction, MIT Press, 1987.

[11] M. Renardy and R.C. Rogers, An Introduction to Partial Differential Equations, Texts in Applied Mathematics, Springer-Verlag, Newyork, 1993.

Table 3. G-filter along x direction.

Case	$G^{(x)}(x,y)$
I $\Delta > 0$	$\frac{2P}{\sqrt{\Delta}} sgn(x)\ a\ b \times$ $[\exp(-a(\lvert x\rvert + \lvert y\rvert)) - \exp(-b(\lvert x\rvert + \lvert y\rvert))]$
II $\Delta < 0$	$K\ sgn(x)\ \exp(-\frac{1}{\sqrt[4]{4P}}\cos(\theta)(\lvert x\rvert + \lvert y\rvert))\times$ $[(\sin(\theta)\varphi - \cos(\theta)\frac{1}{\sqrt[4]{4P}})\cos(\varphi(\lvert x\rvert + \lvert y\rvert))-$ $(\cos(\theta)\varphi + \sin(\theta)\frac{1}{\sqrt[4]{4P}})\sin(\varphi(\lvert x\rvert + \lvert y\rvert))]$
III $\Delta = 0$	$\frac{-1}{4Q^2}\lvert x\rvert\ sgn(x)\ (\frac{1}{\sqrt{Q}}\lvert y\rvert + 1)$ $\exp(-\sqrt{\frac{1}{Q}}(\lvert x\rvert + \lvert y\rvert))$
IV $P = 0$	$-\sqrt{2Q}\ sgn(x)\ \exp(-\sqrt{\frac{1}{2Q}}(\lvert x\rvert + \lvert y\rvert))$

Table 4. Filter types associated with the selected parameter values.

λ	τ 0.0	0.5	1.0
1.0	IV	II	I
8.0	IV	III	I
16.0	IV	I	I

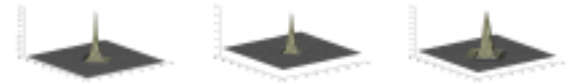

(a) $\lambda = 1.0$

(b) $\lambda = 8.0$

(c) $\lambda = 16.0$

Figure 1. R-filters (τ takes the values $0.0,\ 0.5,$ and 1.0 from left to right).

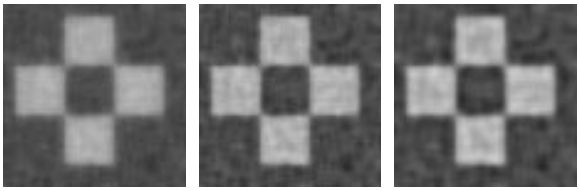

(a) $\lambda = 1.0$

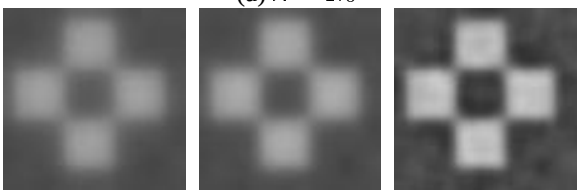

(b) $\lambda = 8.0$

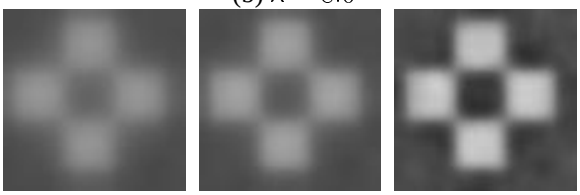

(c) $\lambda = 16.0$

Figure 2. $\lambda\tau$-space representation of Noisy Checkboard Image (τ takes the values $0.0,\ 0.5,$ and 1.0 from left to right).

Table 5. The normalized mean square error (NMSE) between the reconstructed images and the original image.

SNR	λ, τ	Checkerboard 0.0	0.5	1.0	Bars 0.0	0.5	1.0
12dB	1	31.0	**26.8**	29.5	47.5	**35.7**	38.7
	8	54.5	48.5	**35.9**	77.2	74.8	**54.6**
	16	64.2	54.5	**39.5**	84.2	77.7	**60.3**
8.5dB	1	31.8	**28.7**	31.5	48.0	**37.2**	39.8
	8	54.8	48.6	**36.3**	77.3	74.8	**55.0**
	16	65.3	54.5	**39.9**	84.2	77.7	**60.5**
8.5dB	1	32.7	**30.9**	33.6	48.6	**38.9**	41.5
	8	54.9	48.8	**36.9**	77.3	74.8	**55.5**
	16	75.6	54.7	**40.2**	84.2	77.8	**60.9**

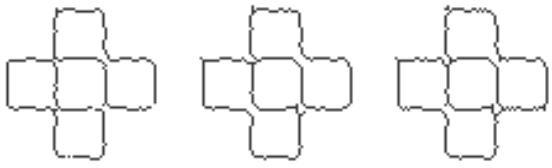

(a) $\lambda = 1.0$

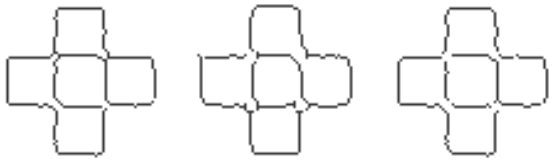

(b) $\lambda = 8.0$

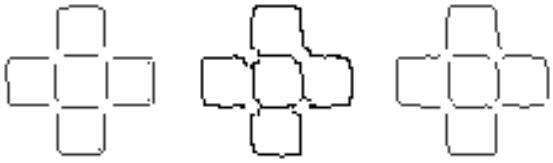

(c) $\lambda = 16.0$

Figure 3. $\lambda\tau$-space representation of edges (τ takes the values $0.0,\ 0.5,$ and 1.0 from left to right).

Figure 4. The original and noisy (SNR=2.4dB) House images.

(a) $\lambda = 1.0$

(b) $\lambda = 8.0$

(c) $\lambda = 16.0$

Figure 5. $\lambda\tau$-space representation of edges for the noisy House image (τ takes the values $0.0,\ 0.5,$ and 1.0 from left to right).

Table 6. Quantitative evaluation of edges from the checkerboard image.

		SNR=12dB			SNR=5dB		
λ	$\tau =$	0	0.5	1	0	0.5	1
1	P(DE/IE)	0.58	0.51	0.52	0.52	0.46	0.46
	P(IE/DE)	0.59	0.50	0.52	0.58	0.52	0.48
	MSD	0.64	0.77	0.75	0.64	0.69	0.75
	FOM	0.60	0.52	0.53	0.53	0.48	0.48
8	P(DE/IE)	0.79	0.73	0.46	0.62	0.57	0.45
	P(IE/DE)	0.81	0.79	0.47	0.63	0.62	0.45
	MSD	0.45	0.49	0.82	0.70	0.82	0.88
	FOM	0.80	0.74	0.49	0.63	0.58	0.47
16	P(DE/IE)	0.79	0.45	0.44	0.73	0.44	0.42
	P(IE/DE)	0.90	0.50	0.48	0.83	0.45	0.45
	MSD	0.36	0.71	0.83	0.57	0.89	0.88
	FOM	0.79	0.47	0.46	0.74	0.47	0.44